Article

Numerical Investigation of Gravity-Driven Granular Flow around the Vertical Plate: Effect of Pin-Fin and Oscillation on the Heat Transfer †

Xing Tian, Jian Yang *, Zhigang Guo and Qiuwang Wang

MOE Key Laboratory of Thermo-Fluid Science and Engineering, Xi'an Jiaotong University, Xi'an 710049, China; tianxing12@stu.xjtu.edu.cn (X.T.); gzgc060811348@stu.xjtu.edu.cn (Z.G.); wangqw@mail.xjtu.edu.cn (Q.W.)
* Correspondence: yangjian81@mail.xjtu.edu.cn; Tel.: +86-29-8266-3502
† This paper is an extended version of our paper published in the 23rd Conference on Process Integration, Modelling and Optimization for Energy Saving and Pollution Reduction, Xi'an, China, 17–21 August 2020; pp. 175–180.

Abstract: In this paper, the heat transfer of pin-fin plate unit (PFPU) under static and oscillating conditions are numerically studied using the discrete element method (DEM). The flow and heat transfer characteristics of the PFPU with sinusoidal oscillation are investigated under the conditions of oscillating frequency of 0–10 Hz, amplitude of 0–5 mm and oscillating direction of Y and Z. The contact number, contact time, porosity and heat transfer coefficient under the above conditions are analyzed and compared with the smooth plate. The results show that the particle far away from the plate can transfer heat with the pin-fin of PFPU, and the oscillating PFPU can significantly increase the contact number and enhance the temperature diffusion and heat transfer. The heat transfer coefficient of PFPU increases with the increase of oscillating frequency and amplitude. When the PFPU oscillates along the Y direction with the amplitude of 1 mm and the frequency of 10 Hz, the heat transfer coefficient of PFPU is increased by 28% compared with that of the smooth plate. Compared with the oscillation along the Z direction, the oscillation along the Y direction has a significant enhancement on the heat transfer of PFPU.

Keywords: gravity-driven granular flow; discrete element method; pin-fin plate; oscillation; heat transfer enhancement

1. Introduction

High-temperature granular matter is widely present in industrial production and energy conversion process; for example, high-temperature particles of more than 1000 K can be produced in the production of cement, lime, coke oven coke, etc. [1]. In addition, granular matter is gradually applied in concentrating solar power [2] and energy storage system [3]. As compared with gas or molten salt [4], granular matter has higher specific heat capacity and higher working temperature [5]. For the heat exchange of high-temperature granular matter, moving bed heat exchangers (MBHE) with low cost, clean energy and wide granularity adaptability are gradually applied to industrial waste heat recovery [6] and concentrating solar power [7]. However, compared with the fluidized bed [8], the heat transfer performance of the MBHE needs to be further improved [9].

In this study, the moving bed heat exchanger is an indirect heat exchanger. Particles are densely filled in the heat exchanger and driven by gravity. Particles exchange heat with horizontal tubes [10] or vertical plates [11] arranged in the heat exchanger. For horizontal tubes, Dai et al. [12] found that a stagnation zone would form at the upstream region of the tube and a cavity zone would form at the downstream region of the tube by experiment, which would seriously affect the flow and heat transfer of particles [13]. Bartsch et al. [14] described these two zones by numerical simulation and verified the simulation results by experiment. Many studies have been carried out to reduce the stagnation zone and the

cavity zone. Liu et al. [15] found that staggered tubes have better heat transfer performance by experiments, and the staggered tubes will strengthen the movement of particles at the top and bottom of the tube. Guo et al. [16] found that the oscillating tube can make the flow of particles in the upstream of the tube more stable, and the particles in the downstream of the tube are in closer contact with the tube wall. Oscillation can significantly improve the heat transfer coefficient. Tian et al. [13] studied the heat transfer of particles flow around the circular tube, the elliptical tube and the flat elliptical tube by discrete element method and found that the shape of the tube had a significant effect on the particle flow at the upstream and downstream of different tubes. The elliptical tube had the smallest stagnation zone and cavity zone, and its heat transfer coefficient was highest. Tian et al. [17] numerically studied the heat transfer of gravity-driven dense particle flow around a hexagonal tube and found that, as the top and bottom angle of the hexagonal tube decreases, the stagnation zone and the cavity zone are reduced, while the heat transfer coefficient is significantly increased. Compared with the horizontal tube heat exchanger, vertical plate heat exchanger has higher heat transfer coefficient due to narrow channels and large surface area. However, thermal gradients will further affect the heat transfer performance [18]. Guo et al. [19] compared the heat transfer characteristics of particles flow around a circular tube and a vertical plate through numerical simulation. They found that particles flow around a vertical plate have better contact with the heat transfer surface and the total heat transfer coefficient of the plate is higher than that of the tube. Natarajan and Hunt [20] experimentally studied the heat transfer between shear and plug flows, and the results show that, at a low flow rate, the average heat transfer coefficients were higher for the shear flows for comparable values of flow velocity close to the wall. Nie et al. [21] analyzed the effects of particles with different thermophysical properties on the performance of the directly irradiated solid particle solar receiver with semi-annular flow channels. Yin et al. [22] found that increasing particle diameter and solid void ratio can reduce the total heat transfer coefficient, and the change of channel width has a great influence on the total heat transfer.

According to the above, most studies focus on the influence of tube arrangement, tube shape, particle properties on heat transfer in MBHE. There are few studies on the enhancement of heat transfer on vertical plate heat exchangers, which have been widely used in concentrated solar power [23]. With the length of the heat transfer surface increasing, the temperature boundary layer of particles moving along the vertical plate develops continuously, and the heat transfer between particles and the plate deteriorates gradually [24]. This paper attempts to enhance the heat transfer of vertical plate heat exchanger by changing the structure of the plate surface on particle side and applying external forces. In this paper, the heat transfer of particle flow around the plate with pin-fin is numerically studied in detail using the discrete element method (DEM). The enhancement effect of pin-fin and oscillation on the heat transfer of particles flow around a vertical plate is investigated. This work will contribute to the design and optimization of MBHE in the future.

2. Method and Simulation

2.1. Method

Particle flow simulation methods can be divided into the continuous method and the discrete method. At present, many scholars simplify the particle flow in the vertical channel as the plug flow [25], regard the particle flow as the continuous medium to simplify the design of MBHE [26] and explore the influence of relevant parameters [22]. When the particles move around a vertical smooth plate, it is feasible to treat the particles as a continuous medium. When there are parts in the flow channel that hinder the movement of particles, the plug flow will be destroyed and the discontinuous movement of particles will be significant; thus, the continuum model is no longer applicable [27]. Compared with the continuous method, the discrete method can calculate the detailed motion of each particle. Nowadays, it has been widely used in the study of particle flow and heat transfer, such as moving bed [13], packed bed [28] and screw reactor [29].

In this paper, DEM based on software EDEM 2.6 is used to simulate the particle flow around the plate with pin-fin. Meanwhile, the self-developed C++ code coupled with DEM is used to solve the heat transfer [18]. The Hertz–Mindlin soft sphere model [30] is used to simulate the particle flow, and the normal force and tangential force between particles are treated by spring, damper, slider and coupler, as shown in Figure 1. The coupler is used to determine the particle pairs in contact. When the tangential force exceeds the yield value, the sliding of the two particles under the action of normal force and friction force is realized through the slider. The contact force is calculated according to the normal overlap and tangential displacement of the particle, and then the motion state of particles is updated. The main heat transfer paths of particles in a slow-moving MBHE are composed of heat conduction inside particles, contact heat conduction, gas heat conduction and radiation. Due to the slow movement of particles and dense filling in the flow channel, the gas convection heat transfer is very small [31], so the gas convection heat transfer is ignored. In addition, radiation is also ignored, while the heat conduction inside the particles, contact heat conduction and gas heat conduction are considered.
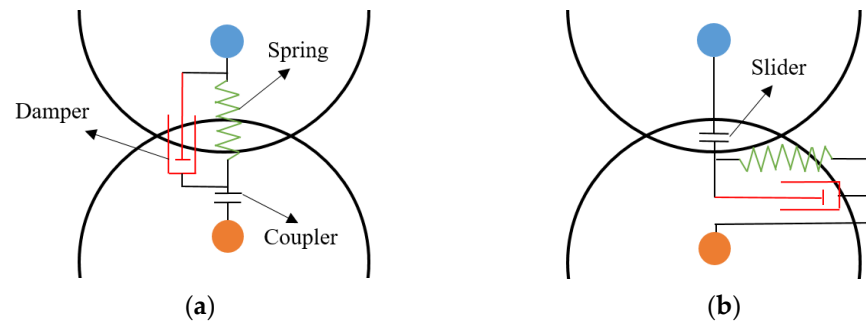

Figure 1. Simplification of the contact force between particles by Hertz–Mindlin soft sphere model: (**a**) normal force; and (**b**) tangential force.

The thermal conduction resistance inside particles (R_1), physical contact thermal conduction resistance (R_2) and thermal conduction resistance through gas film (R_3) are formulated as follows:

$$R_1 = \frac{\sqrt[3]{2} - 1}{2\pi\lambda_s r(1 - \cos\alpha)} \tag{1}$$

$$R_2 = \left[2\lambda_s \left(\frac{3F_n r}{4E_{eq}}\right)^{1/3}\right]^{-1} \tag{2}$$

$$R_3 = \left[\int_\beta^\alpha \frac{2\pi\lambda_g r^2 \sin\theta\cos\theta}{l_{ij} - r\sin\theta - \sqrt{r^2 - (r\sin\theta)^2}} d\theta\right]^{-1} \tag{3}$$

where α is an angle related to the intersection of gas film; β is a starting point angle for the calculation of thermal conduction resistance through gas film; l_{ij} is the distance for the case of particle–particle or particle–wall; λ_g is the thermal conductivity of gas; λ_s is the thermal conductivity of particle; r is the particle radius; F_n is normal direction force; and E_{eq} is Young's modulus.

The overall conduction resistance (R) is presented as follows:

$$R = \begin{cases} R_1 + \frac{R_2 R_3}{R_2 + R_3} + R_1 & \text{Physical contact} \\ R_1 + R_3 + R_1 & \text{Virtual contactt} \end{cases} \tag{4}$$

The heat transfer model adopted in the numerical simulation is based on the following assumptions: (1) The particles in the channel are spherical particles with the same diameter. (2) The heat capacity of the gas is ignored [32], and the temperature of the particle is uniform. (3) The particles are virtually wrapped by the gas film with the thickness of 0.1 dp [33] to establish the heat transfer path in gas phase. (4) The heat transfer path is along the radial direction of the particle. (5) The physical properties of the particles and the gas are kept constant. More details on particle heat transfer model and model verification can be found in the work of Tian et al. [13].

2.2. Model Validations

In the previous study, Tian et al. [18] verified the DEM with heat transfer model in detail through the experimental data [16]. In this paper, an additional case for validating the DEM with heat transfer model is carried out to validate the heat conduction model. The box with a height of 20 d_p is filled with freely packed and stationary spherical particles. The bottom of the box is kept at a constant temperature of 300 K and the initial temperature of the particles is 600 K. The evolution of temperature distribution in the vertical direction of the heat exchange wall at t = 20 s is compared with the temperature distribution calculated by Zehner–Bauer–Schlünder (ZBS) model [34], as shown in Figure 2. The comparison result shows that the temperature field calculated by DEM is in good agreement with that calculated by ZBS model, which indicates that the heat transfer model used in DEM is reasonable.
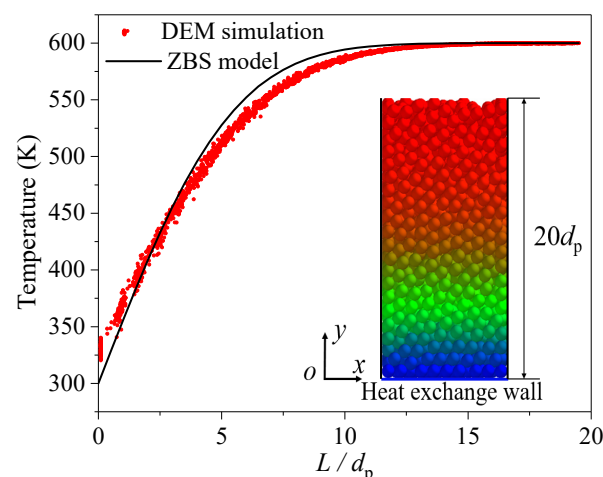

Figure 2. Comparison of temperature distribution with DEM simulation and ZBS model.

2.3. Physical Model and Simulation Cases

The particle side of the vertical flat heat exchanger is uniformly arranged with pin-fin for strengthening heat transfer, as shown in Figure 3a. In this paper, the local effects of pin-fin and oscillations on particle motion and heat transfer are studied. A flat plate with a single pin-fin called the pin-fin plate unit (PFPU) is considered as the simulated geometric model, as shown in Figure 3a. The geometric model used in numerical simulation is shown in Figure 3b. The PFPU is located in the middle of the rectangular channel. The top of the channel is the particle inlet, while the bottom of the channel is the particle outlet. The spherical particles flow in the channel driven by gravity and exchange heat with the PFPU. The dimensions of the rectangular channel are L (length) $\times$ W (width) $\times$ H (height), and the particle diameter (d_p) is fixed at 0.8 mm. PFPU is composed of the plate and pin-fin. The dimensions of the PFPU's plate are H_g (length) $\times$ W_g (width). The pin-fin of PFPU is a cylinder located in the middle of the PFPU's plate, and the side of the cylinder is perpendicular to the plate. The diameter of the pin-fin is D and the length of the pin-fin is L_g, as shown in Figure 3b. Detailed geometric and physical parameters are shown in Table 1.
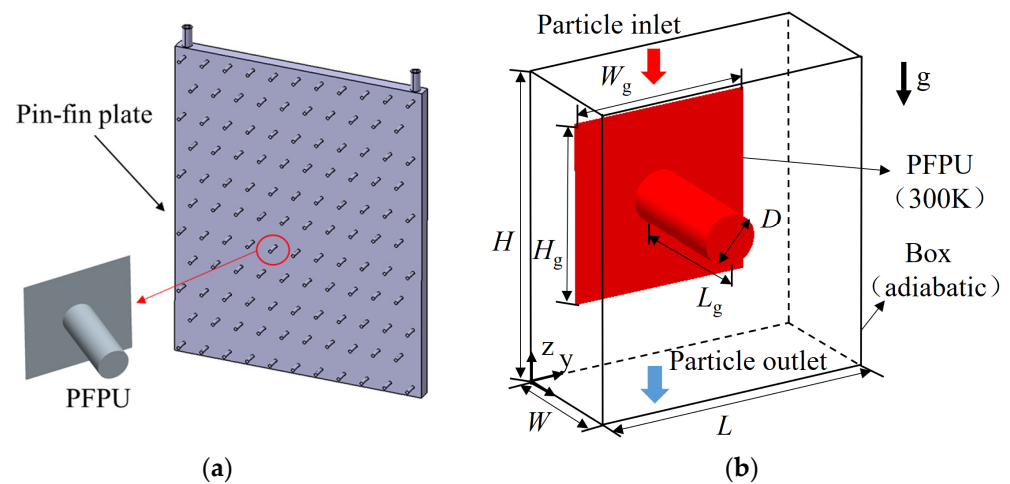
Figure 3. Schematic diagram: (**a**) PFPU; and (**b**) geometry model.

Table 1. Geometric and physical parameters in simulation.

Name	Parameter	Value	Name	Parameter	Value	Name	Parameter	Value
geometry	L (mm)	20	geometry	L_g (mm)	10	particle	ρ (kg/m^3)	2848
	W (mm)	10		W_g (mm)	14		C_p (J/(kg·K))	1210
	H (mm)	20		H_g (mm)	14		λ_p (W/(m·K))	0.55
	D (mm)	4		T_{PFPU} (K)	300		d_p (mm)	0.8
gas	λ_g (W/(m·K))	0.0257	time step	Δt (s)	1.2×10^{-6}		T_{in} (K)	700

During the simulation, the temperature of the PFPU is kept constant at 300 K and the channel wall is adiabatic. The particles with the temperature of 700 K are generated at the inlet of the channel and continuously flow into the channel to ensure the dense filling of particles in the channel. The particle velocity is controlled at the outlet of the channel and keeps constant at −1 mm/s in the Z direction. The parameters related to the calculated motion of particle to particle and particle to wall are shown in Table 2. The whole simulation lasts for 41 s, and the heat Q is analyzed in the last 10 s. The calculation equation for the heat transfer coefficient k of particle flow around PFPU is shown in Equation (5). Q is the total heat between particles and PFPU; A_{PFPU} is the heat transfer area of PFPU; T_{in} is the inlet temperature of particles; T_{PFPU} is PFPU wall temperature; and t is time.

$$k = \frac{Q}{A_{PFPU}(T_{in} - T_{PFPU})\Delta t} \tag{5}$$
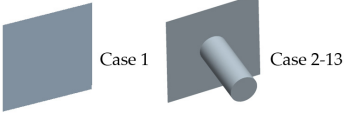
Table 2. The parameters related to the calculated motion of particle to particle and particle to wall.

Mechanical Parameters	Value	Mechanical Parameters	Value
E (particle, Pa)	5.5×10^8	Static friction coefficient (particle–particle)	0.154
E (wall, Pa)	1.82×10^{11}	Rolling friction coefficient (particle–wall)	0.1
Poisson's ratio (particle)	0.25	Rolling friction coefficient (particle–particle)	0.1
Poisson's ratio (wall)	0.30	Restitution coefficient (particle–wall)	0.5
Static friction coefficient (particle–wall)	0.154	Restitution coefficient (particle–particle)	0.3

Particle–particle, the contact between particles; particle–wall, the contact between the particle and the geometrical wall.

In this paper, the heat transfer of PFPU under static and oscillating conditions is numerically studied using DEM. The effects of different amplitudes, oscillating frequencies and oscillating directions on the heat transfer of particles flow around PFPU are investigated. For comparison, the heat transfer of vertical smooth plate with H_g (length) $\times W_g$ (width) is simulated. The oscillation trajectory of PFPU is sinusoidal oscillation, oscillating frequency is 0–10 Hz, amplitude is 0–5 mm (0–1.25 D) and oscillating direction is Y and Z directions. Detailed simulation parameters under different conditions are shown in Table 3. The heat transfer of particles flow around the PFPU is numerically simulated when the oscillation is in the Y direction, the amplitude is 0.25 D and the oscillating frequency varies from 0 to 10 Hz to explore the influence of oscillating frequency. The heat transfer of particles flow around the PFPU is numerically simulated when the oscillating frequency is 3 Hz, the direction of oscillation is Y and Z and the amplitude varies from 0.25 to 1.25 D to explore the influence of the direction and amplitude of oscillation. The heat transfer surface of Case 1 is the smooth plate and the heat transfer surface of Cases 2–13 is PFPU, as shown in Table 3.

Table 3. Simulation parameters for different cases.

Case	1	2	3	4	5	6	Heat Exchange Surface
Oscillating direction	-	-	Y	Y	Y	Y	
Frequency (Hz)	-	0	1	3	5	10	
Amplitude (mm)	-	-	0.25 D	0.25 D	0.25 D	0.25 D	Case 1　　　Case 2-13
Oscillation locus	-	-		Sinusoid			
Case	7	8	9	10	11	12	13
Oscillating direction	Y	Y	Y	Z	Z	Z	Z
Frequency (Hz)	3	3	3	3	3	3	3
Amplitude (mm)	0.5 D	0.75 D	1.25 D	0.25 D	0.5 D	0.75 D	1.25 D
Oscillation locus		Sinusoid			Sinusoid		Sinusoid

3. Results and Discussion

3.1. Effect of Pin-Fin and Oscillation

Cases 1, 2 and 4 are selected to illustrate the influence of pin-fin and oscillation on the heat transfer of particles flow around the plate. The heat exchange surface of Case 1 is the static plate, the heat exchange surface of Case 2 is the static PFPU and the heat exchange surface of Case 4 is the PFPU oscillating in the Y direction. Detailed simulation parameters of Cases 1, 2 and 4 are shown in Table 3. The velocity magnitude distributions of particles flow around different surfaces under different cases are shown in Figure 4. The results show that the particles in Case 1 move at a uniform speed, and there is no relative movement between the particles. In Case 2, the velocity of particles around the pin-fin is significantly different, because the flow channel is impeded by the pin-fin. The velocity of particles at the top of the pin-fin is significantly reduced by the pin-fin. In Case 4, the oscillation of the PFPU in the Y direction intensifies the motion of the particles around the pin-fin, and the particles velocity around the pin-fin is higher than the outlet velocity.
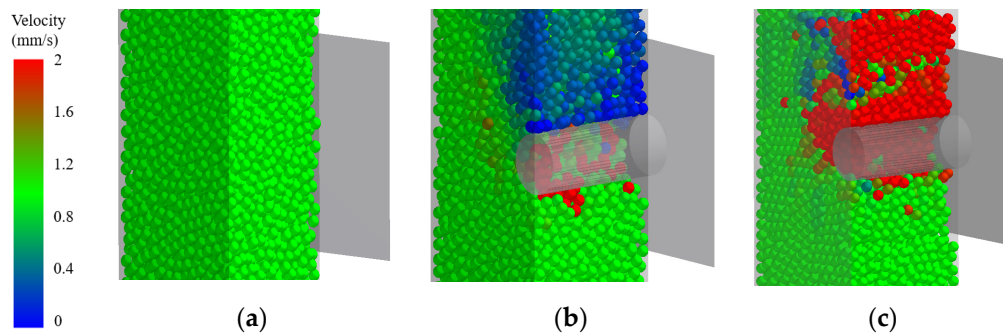
Figure 4. Velocity magnitude distributions of particle flow around different surface under different situation: (**a**) Case 1; (**b**) Case 2; and (**c**) Case 4.

The contact time distributions of particles flow around different surfaces under different cases at *t* = 41 s are shown in Figure 5. The contact time is a cumulative variable, which counts the total time that particles are in contact with the heat exchange surface during the flow process. The distribution and number of particles in contact with the heat exchange surface can be intuitively obtained from the results in Figure 5. In Case 1, only a layer of particles close to the heat transfer surface is in contact with the heat transfer surface, while the particles far away from the heat transfer surface do not contact with the heat transfer surface. In Case 2, due to the addition of the pin-fin, the particles in the middle of the channel can contact the heat transfer surface. In Case 4, the oscillation expands the contact range between the pin-fin and particles, and the number of particles in contact with the heat transfer surface is significantly more than that in Case 2.
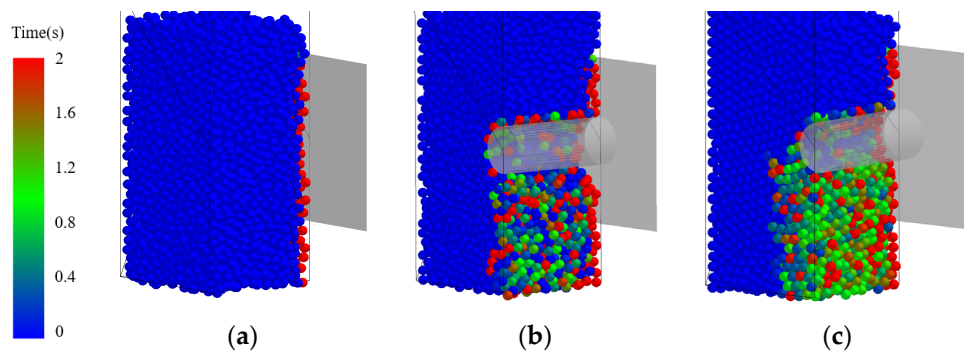

Figure 5. Particle contact time distributions of particle flow around different surface under different situation at *t* = 41 s: (**a**) Case 1; (**b**) Case 2; and (**c**) Case 4.

The time-averaged porosity perpendicular to the wall direction outside the pin-fin is shown in Figure 6a, where *r* is the distance from a point outside the pin-fin to the pin-fin center. Because of the wall effect, the porosity fluctuates regularly near the pin-fin wall region. When particles flow around the static pin-fin in Case 2, the cavity zone is formed below the pin-fin. When the PFPU oscillates along the Y direction in Case 4, the movement of the pin-fin makes the contact between the particles and the pin-fin closer, and the oscillation makes the particle filling rate around the pin-fin increase significantly. Therefore, the porosity of Case 2 is higher than that of Case 4.
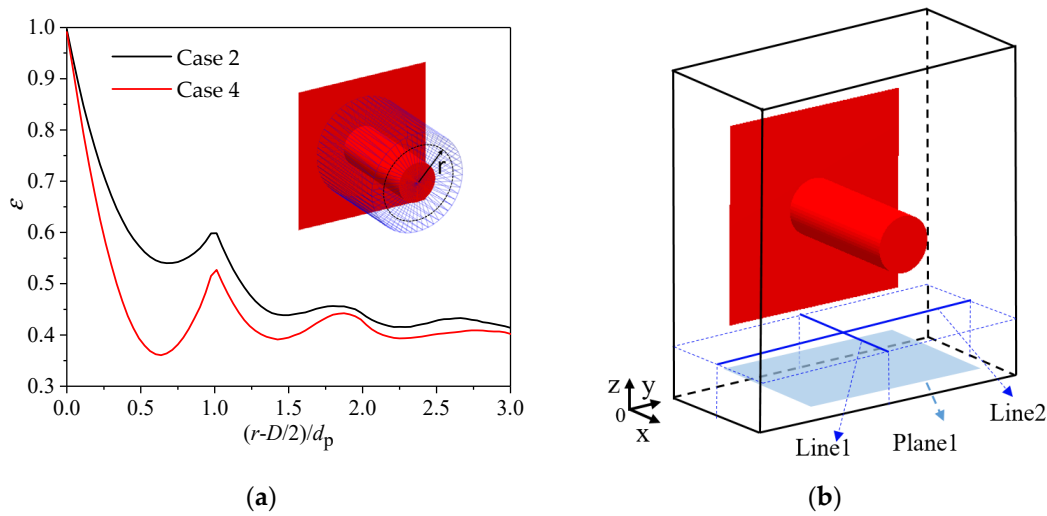
Figure 6. (**a**) Time-averaged porosity outside pin-fin; and (**b**) schematic diagram of Plane 1 and Lines 1 and 2.

The particle temperature distributions at Lines 1 and 2 of t = 41 s are shown in Figure 7. The position of Line 1 is at y = 10 mm and z = 3 mm in the channel. The position of Line 2 is at x = 5 mm and z = 3 mm in the channel, as shown in Figure 6b. Compared with the smooth plate (Case 1), the plate with pin-fin (Case 2) enables particles far away from the plate to exchange heat with the pin-fin, and the temperature of particles at Lines 1 and 2 is significantly lower, as shown in Figure 7a. Compared with the static PFPU (Case 2), the oscillation along the Y direction (Case 4) increases the temperature diffusion of the particle flow around the pin-fin, as shown in Figure 7b.
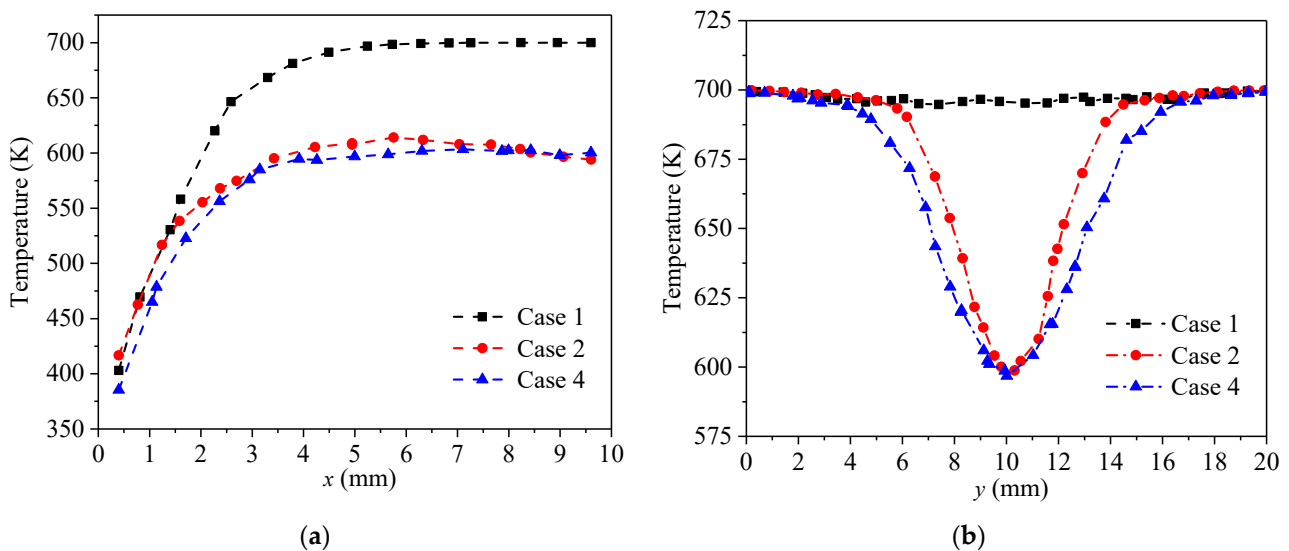

Figure 7. (**a**) Temperature distribution of Line 1 at t = 41 s; and (**b**) temperature distribution of Line 2 at t = 41 s.

The heat transfer characteristics of particles flow around different surfaces under different cases are shown in Table 4. During the simulation time of 21–41 s, the particle contact number with the heat transfer surface is counted. The time-average unit area particle contact number directly describes the contact between particles and the heat transfer surface. The equation of the time-average unit area particle contact number is shown in Equation (6):

$$\nu = \frac{\sum\limits_{\Delta t} N}{A \Delta t} \tag{6}$$

where ν is the time-average unit area particle contact number; N is the number of particles; A is the surface area; and t is the time.

Table 4. Heat transfer characteristics for different cases.

Simulation Cases	1	2	4
Total contact number (N/mm²)	1.31	1.15	1.40
Pin-fin contact number (N/mm²)	-	0.87	1.18
Total Heat transfer rate Φ (W)	14.60	20.94	27.63
Percentage increase of Φ (%)	-	44	89
Pin-fin Heat transfer rate $\Phi_{\text{Pin-fin}}$ (W)	-	8.27	12.38
Heat transfer coefficient k (W/(m²·K))	186	169	224
Percentage increase of k (%)	-	−8.4	21
Particle outlet temperature (K)	656	630	616

The time-average unit area particle contact number of the static PFPU (Case 2) is smaller than that of the smooth plate (Case 1) due to the influence of the cavity zone generated by the particle flow around the pin-fin. When the PFPU oscillates along the Y direction in Case 4, the time-average unit area particle contact number of the pin-fin increases by 35.6% compared with that of the static PFPU in Case 2, and the contact number of the PFPU is higher than that of the smooth plate (Case 1), as shown in Table 4.

Compared with the smooth plate, the area of the PFPU increases by 58%. When the PFPU is static (Case 2), the heat transfer rate of the PFPU increases by 44% compared with the smooth plate (Case 1). Therefore, the heat transfer coefficient of the static PFPU decreases by 8.4% compared with that of the smooth plate (Case 1), as shown in Table 4. When the PFPU oscillates along the Y direction in Case 4, the heat transfer rate of the pin-fin increases by 50% compared with that of the static PFPU in Case 2. Compared with the smooth plate (Case 1), the total heat transfer rate of the oscillating PFPU (Case 4) increases by 89% and the total heat transfer coefficient of the oscillating PFPU (Case 4) increases by 21%, as shown in Table 4. The average temperature of particles in Plane 1 is counted. The position of Plane 1 is in the center of the plane at $z = 1$ mm in the channel, and its length and width are equal to W_{g} and W, respectively. Because the pin-fin makes more particles contact with the heat transfer surface, the average particle temperature at the outlet of PFPU is lower than that of the smooth plate. The outlet temperature of the static PFPU (Case 2) and the oscillating PFPU (Case 4) are 26 and 40 K lower than that of the smooth plate (Case 1), respectively.

3.2. Effect of Frequency

The heat transfer of particles flow around the PFPU is numerically simulated when the oscillation is in the Y direction, the amplitude is 0.25 D and the oscillating frequency varies from 0 to 10 Hz. Detailed simulation parameters are shown in Cases 3–6 in Table 3. The time-average unit area particle contact number of pin-fin and the time-average contact time of particles with pin-fin at different frequencies during the simulation time of 21–41 s are shown in Figure 7a. The equation of the time-average unit area particle contact number is shown in Equation (2). The equation of the time-average contact time is shown in Equation (7):

$$\tau = \frac{\sum\limits_{\Delta t}\sum\limits_{N} t_p}{N\Delta t} \tag{7}$$

where τ is the time-average contact time; t_{p} is the contact time of the particle at the outlet that have been in contact with the heat transfer surface in the flow process; N is the number of particles; and t is the time.

The time-average unit area particle contact number of pin-fin gradually increases with the increase of oscillating frequency, as shown in Figure 8a. When the oscillating frequency of the PFPU is 10 Hz (Case 6), the unit area particle contact number of pin-fin is increased by 40% compared with that of the static PFPU (Case 2). The time-average contact time of particles with pin-fin gradually decreases as the frequency increases. As the oscillating frequency of the PFPU increases, the particles on the surface of the pin-fin update more quickly. When the oscillating frequency of the PFPU is 10 Hz (Case 6), the contact time of particles with pin-fin is reduced by 61% compared with that of the static PFPU (Case 2). The variations of heat transfer coefficient of particles flow around the PFPU at different frequencies are shown in Figure 8b. The heat transfer coefficients of particles flow around the PFPU and pin-fin increase with the oscillating frequency increasing. The heat transfer coefficient of particles flow around the static PFPU is lower than that of particles flow around the plate, while the heat transfer coefficient of particles flow around the oscillating PFPU ($f > 1$ Hz) is significantly higher than that of particles flow around the plate. When the oscillating frequency of the PFPU is 10 Hz (Case 6), the heat transfer coefficient of the particles flow around the PFPU is 28% higher than that of the particle flow around the plate.
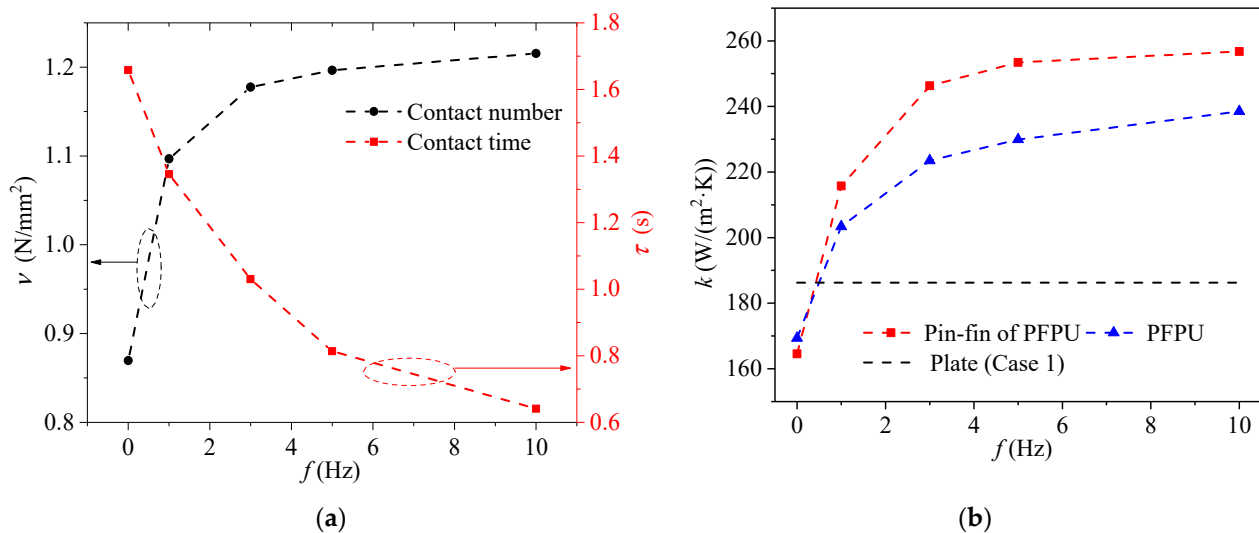

Figure 8. (**a**) Variations of the time-average unit area particle contact number of pin-fin and the time-average contact time of particles with pin-fin at different frequencies ($OD = Y$, $A_\mathrm{m} = 0.25\,D$); and (**b**) variations of heat transfer coefficient of particles flow around the PFPU at different frequencies ($OD = Y$, $A_\mathrm{m} = 0.25\,D$).

3.3. Effect of Oscillating Direction and Amplitude

The heat transfer of particles flow around the PFPU is numerically simulated when the oscillating frequency is 3 Hz, the oscillation is in the Y and Z directions and the amplitude varies from 0.25 to 1.25 D. Detailed simulation parameters are shown in Table 3. The variation of the unit area particle contact number of pin-fin with the amplitude in different oscillating directions is shown in Figure 9a. When the PFPU oscillates along the Z direction, the unit area particle contact number of pin-fin decreases with the amplitude increasing. As the amplitude increases, the cavity zone at the bottom of the pin-fin oscillating along the Z direction gradually increases, and the unit area particle contact number of pin-fin is significantly lower than that of the pin-fin oscillating along the Y direction, as shown in Figure 9a. When the amplitude is 1.25 D, the unit area particle contact number of pin-fin oscillating along the Y direction is increased by 18% compared with that of the pin-fin oscillating along the Z direction. The variation of the contact time of particles with pin-fin with amplitude in different oscillation directions is shown in Figure 9b. With the amplitude increasing, the contact time of particles with pin-fin decreases gradually, and the particle renewal near the pin-fin accelerates. When the amplitude $A_\mathrm{m} < 0.75\,D$, the contact time

of particles with pin-fin along the Z direction is lower than that of the pin-fin oscillating along the Y direction.

The variation of the heat transfer coefficient of particles flow around the PFPU with the amplitude in different oscillating directions is shown in Figure 10. The heat transfer coefficients of particles flow around the PFPU and pin-fin increase with the amplitude increasing. The heat transfer coefficient of the PFPU oscillating along the Y direction is larger than that of the PFPU oscillating along the Z direction. When the PFPU oscillates along the Y direction and the amplitude is 1.25 *D* (Case 9), the heat transfer coefficient of the particles flow around the PFPU increases by 50% compared with that of the particle flow around the plate (Case 1). When the PFPU oscillates along the Z direction and the amplitude is 1.25 *D* (Case 13), the heat transfer coefficient of the particles flow around the PFPU increases by 30% compared with that of the particle flow around the plate (Case 1).
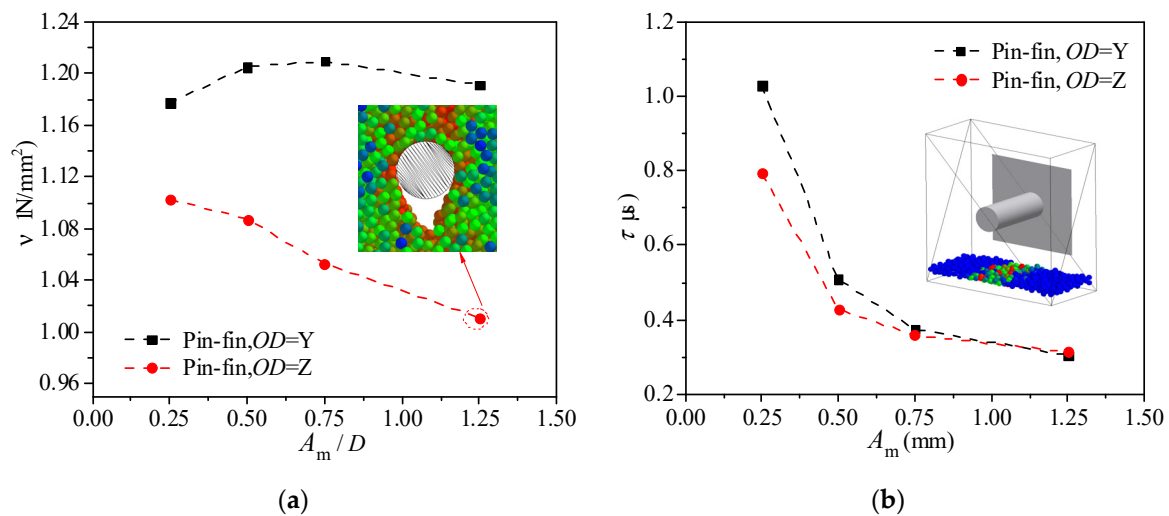
(a)

(b)

Figure 9. (**a**) Variation of the unit area particle contact number of pin-fin with the amplitude in different oscillating directions; and (**b**) variation of the contact time of particles with pin-fin with amplitude in different oscillation directions.
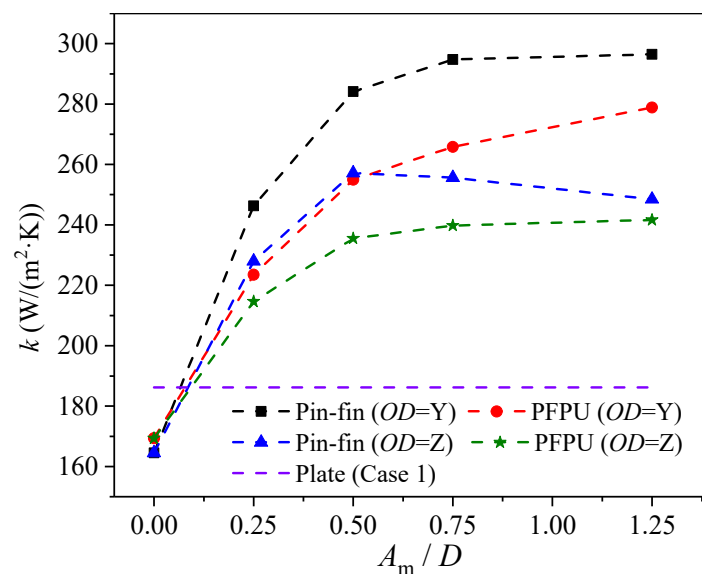

Figure 10. Variations of heat transfer coefficients of particles flow around different surface under different amplitudes.

4. Conclusions

In the present paper, the heat transfer of gravity-driven granular flow around the vertical plate is numerically investigated with DEM, and the enhancements of heat transfer

between vertical plate and particles by pin-fin and oscillation are investigated. The effects of oscillating direction, frequency and amplitude on PFPU are discussed in detail. The main findings are as follows:

(1) Compared with the smooth plate, the area and the heat transfer rate of the PFPU increases by 58% and 44%, respectively. The static PFPU enables particles far away from the plate to exchange heat with the pin-fin, and the average particle temperature at the outlet is lower. When the PFPU oscillates, the number of particles in contact with the PFPU increase significantly, and the particle temperature diffusion around the pin-fin increases. When the PFPU oscillates under the condition of OD = Y, f = 3 Hz and A_m = 0.25 D, the total heat transfer rate and the heat transfer coefficient of the PFPU are increased by 89% and 21%, compared with the smooth plate.

(2) As the oscillating frequency of the PFPU increases, the unit area particle contact number of pin-fin gradually increases, the contact time of particles with pin-fin gradually decreases and the particle renewal near the pin-fin accelerates. When the PFPU oscillates under the condition of OD = Y, f = 10 Hz and A_m = 0.25 D, the unit area particle contact number of pin-fin is increased by 40% and the contact time of particles with pin-fin is reduced by 61%, compared with the static PFPU. The heat transfer coefficients of particles flow around the PFPU increase with the frequency increasing. When the PFPU oscillates under the condition of OD = Y, f = 10 Hz and A_m = 0.25 D, the heat transfer coefficient of the particles flow around the PFPU is 28% higher than that of the particle flow around the plate.

(3) When the PFPU oscillates along the Z direction, the unit area particle contact number of pin-fin decreases with the amplitude increasing and the cavity zone at the bottom of the pin-fin oscillating along the Z direction increases. The unit area particle contact number of pin-fin is significantly lower than that of the pin-fin oscillating along the Y direction. The heat transfer coefficients of particles flow around the PFPU increase with the amplitude increasing. The heat transfer coefficient of the PFPU oscillating along the Y direction is larger than that of the PFPU oscillating along the Z direction. When the PFPU oscillates under the condition of OD = Y, f = 3 Hz and A_m = 1.25 D, the heat transfer coefficient of the particles flow around the PFPU increases by 50% compared with that of the particle flow around the plate.

The present results show that the effect of the pin-fin and vibration on the enhancement of heat transfer is significant, especially the enhancement of vibration perpendicular to the particle flow direction is better. The research in this paper provides more options for the optimization of MBHE, but the economic efficiency of this method and the influence of vibration on the life of heat exchanger still need to be studied in the future.

Author Contributions: Conceptualization, X.T.; Data curation, X.T.; Formal analysis, X.T. and Z.G.; Funding acquisition, J.Y. and Q.W.; Investigation, X.T.; Methodology, X.T.; Project administration, J.Y. and Q.W.; Resources, X.T.; Software, X.T.; Supervision, J.Y.; Validation, X.T.; Writing—original draft, X.T.; and Writing—review and editing, J.Y., Z.G. and Q.W. All authors have read and agreed to the published version of the manuscript.

Institutional Review Board Statement: Not applicable.

Informed Consent Statement: Not applicable.

Data Availability Statement: Not applicable.

Conflicts of Interest: The authors declare no conflict of interest.

Nomenclature

A	Area (mm^2)
A_m	Amplitude (mm)
A_{PFPU}	Area of PFPU (mm^2)
C_{p}	Heat capacity (J/(kg·K))
D	The Pin-fin diameter (mm)
d_{p}	Particle diameter (mm)
E	Young's modulus (Pa)
F_{n}	normal component of the contact force (N)
f	Frequency (Hz)
H	The rectangular channel height (mm)
H_{g}	PFPU's plate height (mm)
k	Heat transfer coefficient (W/(m^2·K))
l	distance of particle–particle or particle–wall (m)
L_{g}	The pin-fin length (mm)
N	Number of particles
OD	Oscillating direction
Q	The total heat between particles and PFPU (J)
r	Radius (mm)
R	thermal resistance (K/W)
T_{in}	The particle inlet temperature (K)
T_{PFPU}	PFPU wall temperature (K)
t	Time (s)
t_{p}	The contact time of the particle (s)
W	The rectangular channel width (mm)
W_{g}	PFPU's plate width (mm)
x,y,z	Cartesian coordinates (mm)
	Greek letters
α, β, Θ	angles (rad)
λ_{g}	Thermal conductivity of gas (W/(m·K))
λ_{p}	Thermal conductivity of particle (W/(m·K))
ν	The time-average unit area particle contact number (N/mm^2)
ρ	Density (kg/m^3)
τ	The time-average contact time (s)
	Abbreviations
DEM	Discrete element method
MBHE	Moving bed heat exchangers
PFPU	Pin-fin plate unit

References

1. Cheng, Z.; Tan, Z.; Guo, Z.; Yang, J.; Wang, Q. Technologies and fundamentals of waste heat recovery from high-temperature solid granular materials. *Appl. Therm. Eng.* **2020**, *179*, 115703. [CrossRef]
2. He, Y.L.; Qiu, Y.; Wang, K.; Yuan, F.; Wang, W.Q.; Li, M.J.; Guo, J.Q. Perspective of concentrating solar power. *Energy* **2020**, *198*, 117373. [CrossRef]
3. Preisner, N.C.; Linder, M. A moving bed reactor for thermochemical energy storage based on metal oxides. *Energies* **2020**, *13*, 1232. [CrossRef]
4. Vignarooban, K.; Xu, X.; Arvay, A.; Hsu, K.; Kannan, A.M. Heat transfer fluids for concentrating solar power systems—A review. *Appl. Energy* **2015**, *146*, 383–396. [CrossRef]
5. Ho, C.K.; Iverson, B.D. Review of high-temperature central receiver designs for concentrating solar power. *Renew. Sustain. Energy Rev.* **2014**, *29*, 835–846. [CrossRef]
6. Cheng, Z.; Guo, Z.; Tan, Z.; Yang, J.; Wang, Q. Waste heat recovery from high-temperature solid granular materials: Energy challenges and opportunities. *Renew. Sustain. Energy Rev.* **2019**, *116*, 109428. [CrossRef]
7. Fang, W.; Chen, S.; Xu, J.; Zeng, K. Predicting heat transfer coefficient of a shell-and-plate, moving packed-bed particle-to-sCO2 heat exchanger for concentrating solar power. *Energy* **2021**, *217*, 119389. [CrossRef]
8. Vogtenhuber, H.; Pernsteiner, D.; Hofmann, R. Experimental and numerical investigations on heat transfer of bare tubes in a bubbling fluidized bed with respect to better heat integration in temperature swing adsorption systems. *Energies* **2019**, *12*, 2646. [CrossRef]

9. Jiang, B.; Xia, D.; Guo, H.; Xiao, L.; Qu, H.; Liu, X. Efficient waste heat recovery system for high-temperature solid particles based on heat transfer enhancement. *Appl. Therm. Eng.* **2019**, *155*, 166–174. [CrossRef]

10. Takeuchi, H. Particles flow pattern and local heat transfer around tube in moving bed. *AIChE J.* **1996**, *42*, 1621–1626. [CrossRef]

11. Fernández-Torrijos, M.; Albrecht, K.J.; Ho, C.K. Dynamic modeling of a particle/supercritical CO_2 heat exchanger for transient analysis and control. *Appl. Energy* **2018**, *226*, 595–606. [CrossRef]

12. Dai, Y.L.; Liu, X.J.; Xia, D. Flow characteristics of three typical granular materials in near 2D moving beds. *Powder Technol.* **2020**, *373*, 220–231. [CrossRef]

13. Tian, X.; Yang, J.; Guo, Z.; Wang, Q.; Sunden, B. Numerical study of heat transfer in gravity-driven particle flow around tubes with different shapes. *Energies* **2020**, *13*, 1961. [CrossRef]

14. Bartsch, P.; Zunft, S. Granular flow around the horizontal tubes of a particle heat exchanger: DEM-simulation and experimental validation. *Sol. Energy* **2019**, *182*, 48–56. [CrossRef]

15. Liu, J.; Yu, Q.; Peng, J.; Hu, X.; Duan, W. Thermal energy recovery from high-temperature blast furnace slag particles. *Int. Commun. Heat Mass Transf.* **2015**, *69*, 23–28. [CrossRef]

16. Guo, Z.; Zhang, S.; Tian, X.; Yang, J.; Wang, Q. Numerical investigation of tube oscillation in gravity-driven granular flow with heat transfer by discrete element method. *Energy* **2020**, *207*, 118203. [CrossRef]

17. Tian, X.; Yang, J.; Guo, Z.; Wang, Q.; Sunden, B. Numerical study of heat transfer in gravity-driven dense particle flow around a hexagonal tube. *Powder Technol.* **2020**, *367*, 285–295. [CrossRef]

18. Guo, Z.; Tian, X.; Tan, Z.; Yang, J.; Zhang, S.; Wang, Q. Numerical investigation of heat resistances in uniform dense granular flows along a vertical plate. *Powder Technol.* **2021**, *385*, 396–408. [CrossRef]

19. Guo, Z.; Tian, X.; Yang, J.; Shi, T.; Wang, Q. Comparison of heat transfer in gravity-driven granular flow near different surfaces. *J. Therm. Sci.* **2020**, *9*, 1–10. [CrossRef]

20. Natarajan, V.V.R.; Hunt, M.L. Heat transfer in vertical granular flows. *Exp. Heat Transf.* **1997**, *10*, 89–107. [CrossRef]

21. Nie, F.; Cui, Z.; Bai, F.; Wang, Z. Properties of solid particles as heat transfer fluid in a gravity driven moving bed solar receiver. *Sol. Energy Mater. Sol. Cells* **2019**, *200*, 110007. [CrossRef]

22. Yin, J.; Zheng, Q.; Zhang, X. Heat transfer model of a particle energy storage-based moving packed bed heat exchanger. *Energy Storage* **2020**, *2*, e113. [CrossRef]

23. Mehos, M.; Turchi, C.; Vidal, J.; Wagner, M.; Ma, Z.; Ho, C.; Kolb, W.; Andraka, C.; Kruizenga, A. *Concentrating Solar Power Gen3 Demonstration Roadmap*; No. NREL/TP-5500-67464; National Renewable Energy Lab (NREL): Golden, CO, USA, 2017; pp. 1–140.

24. Tian, X.; Yang, J.; Guo, Z.; Wang, Q. Numerical study of heat transfer for gravity-driven particle flow along a vertical oscillating pin-fin plate. *Chem. Eng. Trans.* **2020**, *81*, 175–180.

25. Albrecht, K.J.; Ho, C.K. Heat transfer models of moving packed-bed particle-to-sCO2 heat exchangers. *J. Sol. Energy Eng. Trans. Asme* **2019**, *141*, 1–8. [CrossRef]

26. Albrecht, K.J.; Ho, C.K. Design and operating considerations for a shell-and-plate, moving packed-bed, particle-to-sCO$_2$ heat exchanger. *Sol. Energy* **2019**, *178*, 331–340. [CrossRef]

27. Deng, S.; Wen, Z.; Lou, G.; Zhang, D.; Su, F.; Liu, X.; Dou, R. Process of particles flow across staggered tubes in moving bed. *Chem. Eng. Sci.* **2020**, *217*, 115507. [CrossRef]

28. Chen, L.; Wang, C.; Moscardini, M.; Kamlah, M.; Liu, S. A DEM-based heat transfer model for the evaluation of effective thermal conductivity of packed beds filled with stagnant fluid: Thermal contact theory and numerical simulation. *Int. J. Heat Mass Transf.* **2019**, *132*, 331–346. [CrossRef]

29. Qi, F.; Wright, M.M. Particle scale modeling of heat transfer in granular flows in a double screw reactor. *Powder Technol.* **2018**, *335*, 18–34. [CrossRef]

30. Mindlin, R.D.; Deresiewicz, H. Elastic spheres in contact under varying oblique forces. *J. Appl. Mech.* **1953**, *20*, 327–344.

31. Zhang, R.; Yang, H.; Lu, J.; Wu, Y. Theoretical and experimental analysis of bed-to-wall heat transfer in heat recovery processing. *Powder Technol.* **2013**, *249*, 186–195. [CrossRef]

32. Molerus, O. Heat transfer in moving beds with a stagnant interstitial gas. *Int. J. Heat Mass Transf.* **1997**, *40*, 4151–4159. [CrossRef]

33. Chen, R.; Guo, K.; Zhang, Y.; Tian, W.; Qiu, S.; Su, G.H. Numerical analysis of the granular flow and heat transfer in the ADS granular spallation target. *Nucl. Eng. Des.* **2018**, *330*, 59–71. [CrossRef]

34. Zehner, P.; Schlünder, E.U. Thermal conductivity of granular materials at moderate temperatures. *Chem. Ing. Tech.* **1970**, *42*, 933–941. [CrossRef]